Chemical Engineering Journal Advances 26 (2026) 101143

Contents lists available at ScienceDirect

Chemical Engineering Journal Advances

journal homepage: www.sciencedirect.com/journal/chemical-engineering-journal-advances

CO_2 absorption and thermophysical properties of monoethanolamine in choline chloride-ethylene glycol: a solvent for integrated CO_2 capture and electrochemical conversion

Hengameh Farahmandazad *, Nishant Sharma, Iris Burgers, Earl Goetheer, Wiebren de Jong

Section of Large Scale Energy Storage, Department of Process & Energy, Faculty of Mechanical Engineering, Delft University of Technology, Delft, the Netherlands

ARTICLE INFO

Keywords:
Monoethanolamine (MEA)
Ethylene glycol
CO_2 solubility
Reaction mechanism
Heat of absorption

ABSTRACT

Integrating CO_2 capture with electrochemical conversion offers a promising pathway to reduce the energy penalty associated with conventional solvent regeneration. In this context, the development of suitable solvents is crucial. In this study, we develop a non-aqueous Monoethanolamine (MEA)-based solvent composed of Choline Chloride (ChCl) and Ethylene Glycol (EG), designed to function simultaneously as a CO_2 absorbent and an electrolyte in an electrolyzer, thereby eliminating the need for intermediate solvent regeneration steps. Vapor-liquid equilibrium (VLE) measurements were performed to quantify chemical CO_2 absorption, while N_2O was used as an analogue gas to assess the physical CO_2 absorption. Although conventional 30 wt.% aqueous MEA exhibited stronger CO_2 binding at low CO_2 partial pressures ($\leq$1 kPa), our non-aqueous MEA solvent demonstrated markedly higher capacities at moderate to high CO_2 partial pressures (up to 500 kPa), reaching up to 1.2, 1.1, and 0.9 mol CO_2/mol MEA at 25, 40, and 65 °C, respectively, exceeding the theoretical equilibrium limit of aqueous MEA. FTIR spectroscopy identified a transition from predominant carbamate formation at low CO_2 partial pressures to increased carbonate formation derived from EG, together with enhanced physical dissolution at higher CO_2 concentrations, indicating distinct and pressure-dependent reaction pathways. Evaluation of key physical properties, including viscosity, electrical conductivity, and thermogravimetric analysis (TGA), highlighted the critical role of solvent formulation in enabling process integration. While incorporation of ChCl increased viscosity due to its ionic nature, it substantially enhanced thermal stability and provided intrinsic ionic conductivity required for electrochemical operation. Overall, this work demonstrates how solvent composition design in non-aqueous solvent systems enables high CO_2 capacity, tunable reaction chemistry, and electrochemical compatibility, offering a practical pathway toward integrated, energy-efficient carbon capture and utilization technologies.

1. Introduction

Fossil fuel-derived CO_2 emissions are one of the primary causes of global warming and climate change [1]. Atmospheric CO_2 concentrations are increasing by over 2.5 ppm annually, reaching 425 ppm in August 2025 [2]. In response, the 2015 Paris Agreement calls for rapid mitigation of anthropogenic greenhouse gas emissions [3]. Meeting this challenge will require a step change in capture capacity from approximately 40 Mt/year today to about 10 Gt/year by 2070 [4]. To achieve this scale, both carbon capture and storage (CCS) and carbon capture and utilization (CCU) must be deployed across all the industrial sectors.

Amines, particularly in aqueous solutions, are widely employed for post-combustion CO_2 capture from industrial flue gases (4–30 vol.% CO_2) and biogas (40–60 vol.% CO_2) [5]. The CO_2 concentrations in industrial flue gases vary significantly depending on the sector, ranging from about 20–27 vol.% in steel blast furnace gases and 14–33 vol.% in cement processes to more dilute streams such as fired boilers in oil refineries and petrochemical plants (~8 vol.%) and coal-fired boilers (≈12–14 vol.%) [6]. These variations strongly affect the feasibility and energy demand of post-combustion CO_2 capture. In conventional industrial processes, a 30 wt.% (≈ 5 M) aqueous monoethanolamine (MEA) solution is typically used, which absorbs CO_2 at around 40 °C

* Corresponding author at: Leeghwaterstraat 39, 2628 CB Delft, The Netherlands.
E-mail address: h.farahmandazad@tudelft.nl (H. Farahmandazad).

https://doi.org/10.1016/j.ceja.2026.101143

Available online 19 March 2026

through an exothermic reaction. The captured CO_2 is subsequently released via thermal regeneration at 120–140 °C and 1–2 barg, requiring an energy input of about 3–4 GJ/t CO_2. This energy demand accounts for approximately 20–30% of a power plant's output [4]. Despite its fast reaction kinetics and high absorption capacity, aqueous MEA suffers from solvent loss through evaporation, chemical degradation, and corrosion at elevated temperatures, undermining its long-term viability [4,5,7]. These drawbacks motivate the development of solvent designs with higher thermal stability, lower volatility, improved CO_2 selectivity, and reduced regeneration energy requirements.

One of the carbon capture and utilization approaches is the direct integration of CO_2 capture with electrochemical conversion in a single unit operation. In this concept, a single liquid medium functions simultaneously as the CO_2 absorbent and as the electrolyte in the electrolyzer. In this integrated approach, the energy-intensive thermal desorption step is replaced by electrochemical process, where in-situ CO_2 release and conversion (e.g., to syngas) occurs directly in the electrolyzer. It is important to note that in large-area electrochemical stack cells, ohmic losses inherently generate heat which elevates operating temperatures (≈ 40–70 °C). This internally generated heat can be advantageously utilized to facilitate in-situ CO_2 desorption, thereby reducing the overall energy demand of the process [8,9].

Successful implementation of this integrated capture-conversion approach strongly depends on the design of suitable solvent that can simultaneously support efficient CO_2 absorption, adequate electrical conductivity, and electrochemical stability. Amines, particularly MEA, represent promising candidates because of their well-established role in industrial CO_2 capture. In this integrated configuration, mixtures of amines with appropriate non-aqueous co-solvents offers several advantages over conventional aqueous solvents, enabling both desorption and electrochemical conversion within a single process unit. Low-volatility organic co-solvents can significantly reduce the energy required for solvent regeneration. For instance, ethylene glycol (EG) has a vapor pressure of 0.007 kPa (at 20 °C) and a normal boiling point of 197.1 °C (at 1 atm) [10–12].

Beyond reducing regeneration energy, non-aqueous co-solvents for MEA can enhance the physical solubility of CO_2, while still supporting chemical absorption [4]. Here, two solvent interaction properties are particularly important:

(i) Physical dissolution of CO_2, which depends on the solvent's dielectric constant (ε) and Hildebrand solubility parameter (δ) [13,14]. Lower ε values and moderate δ values favor higher physical CO_2 solubility [11]. Excessively high δ values indicate strong solvent-solvent cohesion, which can hinder CO_2 dissolution [15].

(ii) Chemical stabilization of CO_2-amine adducts. Once CO_2 reacts with the amine, carbamate or other intermediate species are formed. The stability of these ionic intermediates requires sufficiently higher ε values to stabilize charged species [16].

Therefore, an optimal balance between ε and δ is essential. A moderate dielectric constant combined with an appropriate cohesive energy density can enhance both physical and chemical CO_2 absorption. Leites et al. [16] reported that co-solvents for MEA with $\varepsilon > 23$ act as effective diluents for MEA, supporting efficient CO_2 capture performance [16]. For instance, EG has a dielectric constant of 37.7 (at 25 °C) [10,17], whereas water exhibits a much higher value of approximately 80 (at 20 °C and 1 bar) [18]. Similarly, the Hildebrand solubility parameter for EG is 29.9 $MPa^{1/2}$, while for water, it is 47.9 $MPa^{1/2}$ [19].

Among non-aqueous co-solvents, ionic liquids (ILs) and deep eutectic solvents (DESs) stand out for high thermal and electrochemical stability, structural tunability, and favorable CO_2 selectivity [19–23]. DESs, formed from a hydrogen-bond acceptor (HBA) and donor (HBD), are greener, lower-cost, and easier to synthesize alternatives to ILs. They form mixtures with melting points below those of their individual components [21,22,25]. Their viscosity, conductivity, and physical CO_2 solubility can be tuned by adjusting the component selection and composition [22]. Within this type of solvents, choline chloride (ChCl): EG mixtures, especially at a 1:2 molar ratio with $\delta \approx 24.5$ MPa½ [14], have been widely investigated for physical CO_2 capture and electrochemical reduction due to their low viscosity, high conductivity, and chemical robustness [25–31]. Although these mixtures are often classified as DESs, some studies suggest they are more accurately described as DES-analogues, with the true eutectic point near ≥ 1:4.85 molar ratio (ChCl:EG) [33]; nonetheless, mixtures below this threshold retain tunable, DES-like physicochemical behavior [30].

Each component of the ChCl:EG mixture offers its own distinct advantages. As noted above, EG provides favorable properties for CO_2 capture, with CO_2 being more soluble in pure EG than in water at 298 K [32,34]. ChCl is biodegradable and non-toxic and can enhance CO_2-to-CO electrocatalysis by modifying Ag surfaces, stabilizing intermediates, and improving the local reaction environment [24,34–37]. ChCl also increases the thermal stability of the EG at elevated temperatures [38]. In amine-based solvents, adding EG to MEA-containing mixture mitigates the sharp viscosity increase typically observed after CO_2 uptake, maintains absorption efficiency, and minimizes solvent loss during regeneration due to the high boiling point of EG [39]. Importantly, ^{13}C NMR analysis further confirms that regenerated MEA-EG-containing mixture retain the same structural features as fresh mixture, indicating good solvent stability and recyclability [39].

To quantify the relative contributions of the solvents to physical CO_2 absorption, the nitrous oxide (N_2O) analogy method is commonly employed [40]. N_2O closely resembles CO_2 in molecular weight, linear geometry, and Henry's law constants and is therefore widely recognized as a reliable representation for evaluating physical CO_2 solubility in amine solvents [41]. Unlike CO_2, N_2O does not chemically react with amines; therefore, comparing CO_2 and N_2O absorption enables the distinction of physical solubility from chemical absorption [34].

In addition, the reduced water content in integrated capture-conversion processes help to suppress the hydrogen evolution reaction (HER) during CO_2 electrolysis, thereby improving selectivity for the CO_2 reduction reaction (CO_2RR) [4]. Nevertheless, other properties such as viscosity, electrical conductivity, and thermal stability are equally important for overall process performance and scale-up [24,42].

Building on our previous findings, we demonstrated the viability of using ChCl:EG as a catholyte in CO_2 electrolysis, optimizing its composition across various mol ratios (1:x, x = 2, 3, 4) [35]. More recently, we incorporated 0.5 M (≈ 3 wt.%) MEA into ChCl:EG (1:4 mol ratio) to enhance CO_2 solubility through chemical absorption and evaluated its performance in an electrolyzer operating at elevated temperature (~65 °C) [43]. This novel solvent exhibited dual functionality, acting simultaneously as a CO_2 absorbent and as an electrolyte, marking a significant step toward integrated capture and conversion processes.

Having established proof of concept, the next step is to assess the solvent's suitability for integrated CCU by examining its thermophysical properties and absorption mechanisms. In this study, we comprehensively investigated 0.5 M MEA in ChCl:EG (1:4 mol ratio), with emphasis on properties critical for an integrated processes. A systematic experimental workflow was therefore designed to link CO_2 absorption performance, molecular reaction pathways, physical transport behavior, and thermal stability. The complete methodology and experimental sequence are described in Section 2.3.

2. Methodology

2.1. Chemicals

All chemicals were purchased from commercial suppliers and used without further purification: choline chloride (≥98%, Sigma-Aldrich), ethylene glycol (≥99.5%, for analysis, EMSURE), monoethanolamine

(≥98%, Sigma-Aldrich). The chemical structures of the individual components in the solvent mixture are illustrated in Fig. 1. Potassium bicarbonate ($KHCO_3$) (≥99.5% trace metals basis, Sigma-Aldrich) was used as a reference standard for bicarbonate solution in the FTIR measurements. High purity CO_2 gas (grade 5, Linde Gas Benelux B.V.) was used for the experiments and measurements.

2.2. Solvent preparation

ChCl and EG were prepared at mol ratios of 1:2, 1:3, and 1:4 by accurately weighing the components according to the desired mol ratios. In each case, one mol of ChCl was combined with 2, 3, or 4 mol of EG, respectively [35]. The components were transferred into sealed laboratory glass bottles (Laboratory Bottles, VWR®), mixed and heated to 80 °C with gentle stirring for 2 h until a clear and colorless homogeneous liquid was formed [35]. For the amine-based solvent, MEA was added to the prepared ChCl:EG mixture to achieve concentrations of 0.5, 3, 6, and 9 M and stirred at 70 °C for 2 h [43]. All solvents were stored under vacuum to prevent moisture contamination.

2.3. Experimental workflow

To evaluate the suitability of the non-aqueous MEA-ChCl-EG solvent for an integrated CO_2 capture and electrochemical conversion, a systematic experimental workflow was designed to link CO_2 absorption performance, molecular reaction pathways, physical transport properties, and thermal stability. The characterization techniques shown in Fig. 2 were implemented sequentially to provide a comprehensive assessment of solvent functionality within an integrated capture-conversion framework.

The workflow begins with vapor-liquid equilibrium (VLE) measurements to quantify CO_2 solubility over a wide pressure range (up to 500 kPa) at 25, 40, and 60 °C, alongside a validation against 30 wt.% aqueous MEA. The N_2O analogy method was applied to distinguish physical from chemical absorption contributions, and the heat of absorption was estimated using the Clausius-Clapeyron approach. Molecular-level reaction pathways were subsequently investigated using FTIR spectroscopy under controlled CO_2 loadings to identify carbamate and carbonate formation, consistent with mechanisms previously validated by complementary NMR-FTIR studies reported in the literature.

Physical transport properties relevant to capture and electrochemical operation, including viscosity and electrical conductivity, were evaluated under both CO_2-loaded and unloaded conditions across temperature range 20–60 °C. Finally, thermogravimetric analysis (TGA) was conducted to assess thermal stability and operational robustness at elevated temperatures.

Characterization measurements were performed over a temperature range of 20–60 °C, and VLE experiments were specifically conducted at 25, 40, and 65 °C to reflect realistic operating conditions of the integrated CO_2 capture and electrochemical conversion process, as detailed in our previous work [43]. The upper temperature of 65 °C was selected based on electrochemical operating constraints [43]. In the integrated process, CO_2 is desorbed in-situ within the electrolyzer and simultaneously reduced to CO. Industrial-scale CO_2 electrolyzers typically operate within 40–70 °C due to heat generation from overpotentials, ohmic losses, and reaction enthalpy, particularly near the catalyst layer. Thus, 65 °C represents a realistic upper-bound operating condition. Additionally, this temperature remains within the thermal stability limit of the Nafion N117 membrane used in this electrochemical conversion process, which begins to degrade above ~ 80 °C. Higher temperatures were therefore avoided to ensure stable membrane performance and electrochemical operation [43]. An intermediate temperature of 40 °C was chosen to approximate typical flue gas temperatures entering industrial absorbers in post-combustion capture processes [5]. The lower temperature of 25 °C was included as a reference condition, enabling benchmarking under near-ambient conditions where CO_2 solubility is generally higher [6]. Together, these temperatures enable evaluation of solvent performance across practical absorption and electrochemical operating windows relevant to process integration.

2.3.1. CO_2 and N_2O solubility measurements (VLE)

The VLE setup consists of a 1000 ml stainless-steel vessel equipped with gas and liquid phase stirring. It operates from ambient temperature up to 150 °C and pressures up to 6 bar. Three pressure transducers (P-30, WIKA) cover ranges up to 0.4 bar, 2.5 bar, and 6 bar. At low pressures, the accuracy of the measurements is limited by the sensitivity of the pressure transducers. Temperature is controlled using an oil-circulating bath and a heating jacket. The temperatures of both the liquid phase and the headspace are continuously monitored using PT100 resistance thermometers. The heating jacket covers the vessel and tubing, except for the vessel's circular window for visual observation. A mass flow controller (FG-201CV, Bronckhorst) regulates and monitors the gas flow (CO_2 or N_2O). All operations are automated and monitored through LabVIEW software. The VLE experimental setup used in this study to measure the CO_2 solubility is shown in Figure S2, while Figure S3 presents the complete piping and instrumentation diagram (P&ID), highlighting the main components of the solvent. To validate the reliability and accuracy of the VLE setup, benchmark experiments were conducted using a 30 wt.% aqueous MEA solution under identical conditions, as reported in the Supporting Information. The measured CO_2 loading values show excellent agreement with well-established literature data, as illustrated in Figure S4.

A 400 ml sample of the prepared solvent was first degassed in an ultrasonic bath for 20 min at ambient temperature and then transferred to the sealed vessel. The system was purged with N_2 to remove air, evacuated, and heated to the desired temperature (25, 40, and 65 °C). Gas (CO_2 or N_2O) was introduced stepwise under automated control until the target pressure (6 bar) or step count was reached. The number of steps and the amount of gas added per step were defined through LabVIEW software.

The step time refers to the time interval between consecutive gas (CO_2 or N_2O) dosing steps and the equilibration period. At each step, a defined and identical amount of gas was injected into the vessel, and the system was allowed to reach equilibrium before the next dosing step begins. Thus, the step time includes both the gas injection and the equilibration period. Continuous stirring was maintained throughout to enhance gas absorption. Equilibrium was assumed once the pressure stabilized, and the corresponding equilibrium pressure (p_{gas}) was then calculated:

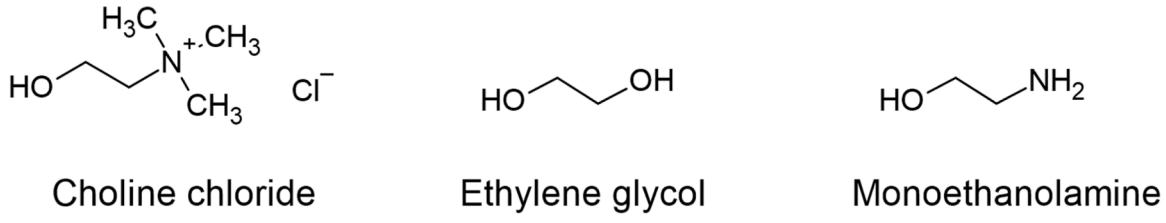

Fig. 1. The chemical structures of the individual components in the solvent mixture, 0.5 M MEA in ChCl:EG (1:4 mol ratio).

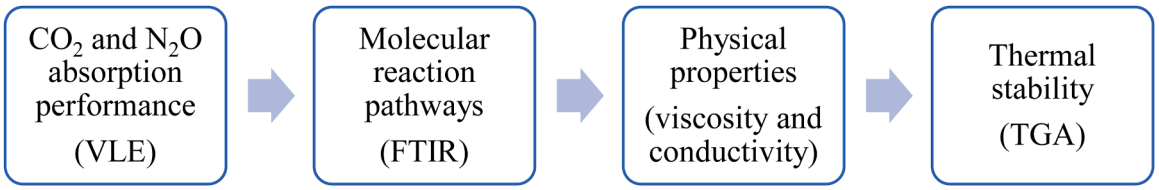

Fig. 2. Schematic of the experimental workflow for evaluating the non-aqueous MEA-ChCl-EG solvent in an integrated CO_2 capture and electrochemical conversion process.

$$p_{gas} = P_{total} - P_{start} \quad (1)$$

where, P_{start} (Pa) is the vapor pressure of the solvent at the studied temperature (no CO_2 or N_2O yet). Under the recorded temperature and pressure conditions, the volume of the vapor phase was determined from the known volumes of the solvent and the vessel. Using this vapor volume as input, the amount of CO_2 or N_2O present in the gas phase was calculated based on the Ideal Gas Law (Eq. (2)). Furthermore, the total amount of gas introduced was obtained from the mass flow controller readings, allowing for the determination of the amount of gas dissolved in the liquid phase.

$$n_{gas} = \frac{p_{gas} V_{gas}}{RT} \quad (2)$$

where, n_{gas} is the number of moles of CO_2 or N_2O absorbed in the liquid phase (mol); V_{gas} is gas-phase volume (m^3); T is absolute temperature (K); R is the universal gas constant (8.314 J/mol·K).

The CO_2 loading (α) was then calculated as:

$$\alpha = \frac{n_{gas}}{n_{amine}} \quad (3)$$

For N_2O, Henry's constant was calculated as:

$$H_{N_2O} = \frac{p_{N_2O}}{C_{N_2O}} \quad (4)$$

where, H is Henry's constant of N_2O in the mixture ($Pa.m^3/mol$); pN_2O is equilibrium partial pressure of N_2O (Pa); and CN_2O is the concentration of N_2O in the liquid phase (mol/m^3).

Assuming purely physical absorption, a linear relationship between partial pressure and concentration is expected. Experimental solubility data as a function of temperature were fitted to an exponential model:

$$H = Ae^{\frac{B}{T}} \quad (5)$$

where, T is absolute temperature (K); and A, B are adjustable parameters.

Determination of Heat of CO_2Absorption

At equilibrium, the chemical potential of CO_2 in the gas phase equals that in the liquid phase. For a given CO_2 loading, the equilibrium gas-phase partial pressure (pCO_2) varies with temperature. This temperature dependence provides a way to estimate the heat associated with the absorption process. The Clausius-Clapeyron equation is commonly used to describe how vapor pressure changes with temperature, and it can be adapted to determine the heat of absorption (ΔH_{abs}) in CO_2 absorption:

$$\ln(p_{CO2}) = -\frac{\Delta H_{abs}}{R}\frac{1}{T} \quad (6)$$

where, pCO_2 is the equilibrium CO_2 partial pressure (Pa); T is absolute temperature (K); R is the universal gas constant (8.314 J/mol·K); and ΔH_{abs} is the heat of absorption (J/mol).

For each fixed CO_2 loading, equilibrium pressure were measured at 25, 40, and 65 °C. A plot of $\ln(pCO_2)$ vs. T results in a straight line. The slope of this line corresponds to $-\Delta H_{abs}/R$ which determines the heat of absorption. Linear regression was applied to the three measured temperature points for each loading. Reproducibility between two independent experimental datasets at each loading was evaluated. The combined uncertainty (±σ) was obtained by summing the regression and reproducibility contributions in quadrature, as reported in Figure S10 and Table S5.

2.3.2. FTIR spectroscopy

Fourier-transform infrared (FTIR) spectra were recorded using Nicolet™ iS50 (Thermo Scientific™) equipped with ATR diamond crystal. Measurements were performed at room temperature over the wavenumber range of 4000–400 cm^{-1} with a resolution of 4 cm^{-1} and averaging 32–64 scans per sample to improve signal to noise ratio. Samples were analyzed under both CO_2-loaded and unloaded conditions to monitor structural changes and identify functional groups associated with absorption mechanisms. A fully CO_2-loaded solution was prepared using the CO_2 loading setup (Figure S1) by equilibrating the solvent with CO_2 at 1 bar and room temperature. This condition was defined as 100% CO_2 loading (fully CO_2-loaded solution).

To identify the FTIR spectral changes upon different CO_2 absorption, the fully CO_2-loaded solution was then subsequently serially diluted with the unloaded solvent to obtain samples corresponding to 0%, 20%, 40%, 60%, and 80% CO_2 loading.

2.3.3. Physical property measurements

Viscosity measurements were carried out using a modular compact rheometer (MCR 302, Anton Paar) in the temperature range of 20–60 °C. Temperature control was provided by a Peltier control system (PTD, –40 to 200 °C) coupled with a water-circulating bath for counter-cooling/heating, ensuring stable thermal conditions. Measurements were performed using a measuring plate (PP50, 50 mm diameter) with defined geometry under controlled shear-rate conditions. Each viscosity value represents the average of 21 data points, and all measurements were performed in duplicate. Electrical conductivity was determined using a 914 pH/conductometer (Metrohm) with an accuracy of ±1% in the range of at 1mS to 500 mS.

2.3.4. Thermal stability analysis (TGA)

Thermal stability of the solvents was evaluated using a thermogravimetric analyzer (SETARAM TAG 1750). Approximately 0.5 ml of each sample was placed in platinum-alumina crucibles. Thermograms were recorded over the temperature range of 25–150 °C at a heating rate of 3 °C/min under an argon atmosphere. Data analysis was performed using Universal Analysis software to identify key thermal characteristics, including mass loss (wt.%), and the onset, peak, and final temperatures associated with melting and boiling transitions.

3. Results and discussions

3.1. CO_2 and N_2O solubility: chemical and physical absorption

To distinguish chemical and physical absorption, we compared CO_2 and N_2O solubility at 25, 40, and 65 °C, using N_2O as a non-reactive analogue for physical absorption. The VLE data provide a comprehensive assessment of the performance of our proposed solvent, 0.5 M MEA in ChCl:EG (1:4 mol ratio), compared with the benchmark 30 wt.% aqueous MEA (Table S1-S3).

3.1.1. CO_2 solubility

Fig. 3 and Table S1 present the VLE data for CO_2 in our proposed solvent over a range of CO_2 partial pressures of 0.03 to 550 kPa at 25, 40, and 65 °C. As expected, increasing CO_2 partial pressure significantly increases CO_2 loading until the solvent approaches saturation. Because the amine-CO_2 absorption reaction is exothermic, lower temperatures promote stronger binding and greater CO_2 uptake (25 °C > 40 °C > 65 °C). Conversely, increasing temperature promotes desorption by shifting the equilibrium back toward CO_2 release.

At low CO_2 partial pressures, 30 wt.% aqueous MEA exhibits stronger binding affinity for CO_2 and maintains CO_2 loading below 0.5 mol CO_2/mol MEA. However, at moderate to high CO_2 partial pressures, the non-aqueous MEA solvent shows substantially higher CO_2 absorption capacity, reaching up to 1.2, 1.1, and 0.9 mol CO_2/mol MEA at 25, 40, and 65 °C, respectively. These loadings far exceed the theoretical equilibrium limit of 0.5 mol CO_2/mol MEA typically observed for 30 wt.% aqueous MEA.

This theoretical equilibrium capacity originates from the carbamate formation mechanism in aqueous MEA solvents, where each CO_2 molecule reacts with one MEA molecule via a zwitterion intermediate that subsequently protonates to form carbamate. The resulting 2:1 MEA-to-CO_2 stoichiometry (Reaction 3) restricts the equilibrium loading to 0.5 mol CO_2/mol MEA. At loadings above 0.5, aqueous MEA solutions begin to form bicarbonate through CO_2 hydration and carbamate hydrolysis, a pathway that are strongly facilitated by the presence of water [44].

In contrast, the enhanced CO_2 uptake ($\alpha > 0.5$) observed in the non-aqueous MEA indicates the presence of additional absorption mechanisms beyond the conventional carbamate pathway. This elevated uptake likely results from a combination of enhanced physical CO_2 solubility in the ChCl:EG solvent and alternative chemical reaction pathways.

To distinguish between these contributions and identify the origin of the higher CO_2 capacity, N_2O solubility measurements were conducted as an analogue to quantify the physical absorption component. In parallel, FTIR spectroscopy was employed to identify reaction products and probe molecular-level changes in the solvent. The spectral interpretation was further supported through comparison with previously reported studies that used complementary NMR-FTIR analyses, where NMR confirmed species formation and FTIR tracked functional group evolution. This combined approach enables a clearer understanding of the mechanisms responsible for the superior CO_2 uptake observed in the non-aqueous solvent compared to aqueous MEA solvents.

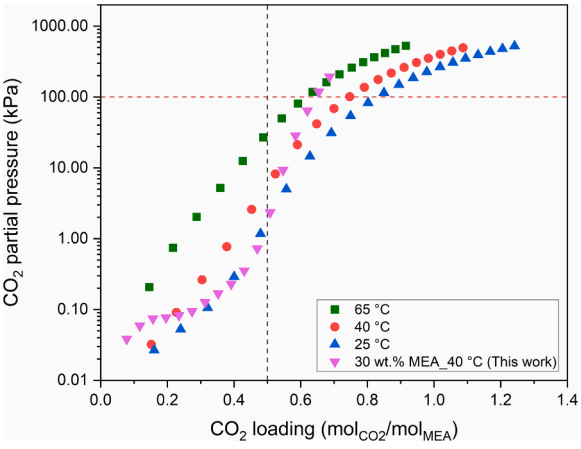

Fig. 3. Comparison CO_2 VLE isotherms for 0.5 M MEA in ChCl:EG (1:4 mol ratio) at 65 °C (green), 40 °C (red), and 25 °C (blue), and for 30 wt.% aqueous MEA at 40 °C (purple).

3.1.2. N_2O solubility

To estimate the physical contribution to CO_2 uptake, N_2O solubility was measured and the results are presented in Fig. 4a and Table S3. These results highlight the temperature-dependent solubility behavior of N_2O in the solvent. At 25 °C, N_2O shows the highest solubility, whereas at 65 °C, the solubility is significantly reduced.

Moreover, the linear pressure-concentration relationship observed at all three temperatures shown in Fig. 4b indicates that Henry's Law is applicable within the studied pressure range. Henry's constant increases from approximately 3.7 to 6.1 kPa·m^3/mol N_2O as temperature rises, reflecting reduced gas solubility at higher temperatures.

To compare CO_2 and N_2O on the same basis, CO_2 loadings were converted to mol CO_2/kg solvent, and N_2O solubility was interpolated to corresponding CO_2 pressures. Physical CO_2 solubility was estimated by applying a correction factor of 1.29 (from Oyevaar et al.) [34], based on CO_2/N_2O solubility ratios in pure EG at 298 K. Although the ChCl:EG mixture likely exhibits higher CO_2 solubility than pure EG, this assumption provides a reasonable estimate in the absence of detailed experimental data for the ChCl:EG mixture. We also assumed that MEA primarily contributes to chemical absorption, with a negligible effect on the physical absorption of CO_2.

By subtracting the estimated physical absorption from the total CO_2 solubility, the chemical contribution to CO_2 uptake is isolated, as illustrated in Fig. 5a. Although physical absorption plays a role to the overall uptake, chemical absorption clearly dominates, with values exceeding the theoretical equilibrium capacity MEA capacity (0.5 mol CO_2/mol MEA) expected for the carbamate formation.

This observation indicates that additional chemical interactions beyond the conventional carbamate pathway must occur in the non-aqueous solvent environment through the CO_2 uptake. In particular, the presence of the ChCl:EG medium enables alternative reaction pathways or stabilize additional CO_2-derived species, thereby increasing the overall absorption capacity. To elucidate the molecular origin of this enhanced CO_2 uptake, FTIR spectroscopic analysis is discussed.

3.2. Reaction pathways and speciation by FTIR

In this study, FTIR spectroscopy was employed to monitor and identify structural and speciation changes in the solvent before and after CO_2 absorption. The obtained spectra were interpreted in the context of well-established literature that combined complementary NMR and FTIR analyses, where NMR confirmed species formation while FTIR tracked functional group evolution. This combined interpretation provides reliable support for the proposed reaction pathways.

To obtain a clearer spectral distinction and a deeper understanding of the interactions among solvent components, FTIR spectra of the individual components, including ChCl, EG, and MEA, were first recorded (Figure S5a). Subsequently, spectra of the mixtures with varying compositions and upon CO_2 loading were collected (Figure S5b-c).

The reaction mechanism of CO_2 with non-aqueous MEA generally involves the formation of a zwitterion intermediate, which subsequently reacts with an additional MEA molecule to form an MEA carbamate ($MEACOO^-$) and protonated MEA ($MEAH^+$) [41]:

$$CO_{2(l)} + MEA \rightleftharpoons MEAH^+COO^- \quad \text{(Reaction 1)}$$

$$MEAH^+COO^- + MEA \rightleftharpoons MEACOO^- + MEAH^+ \quad \text{(Reaction 2)}$$

The overall reaction can be expressed as:

$$CO_{2(l)} + 2MEA \rightleftharpoons MEACOO^- + MEAH^+ \quad \text{(Reaction 3)}$$

To confirm the formation of these species in our solvent, comparative FTIR analyses were performed on ChCl:EG mixtures with and without MEA and CO_2 (Figs. 6a-b and S5b-c). As shown in Fig. 6a, introducing CO_2 into MEA-ChCl:EG (1:4 mol ratio) mixtures at various MEA concentrations (0.5 M, 3 M, and 9 M) resulted in distinct spectral changes at

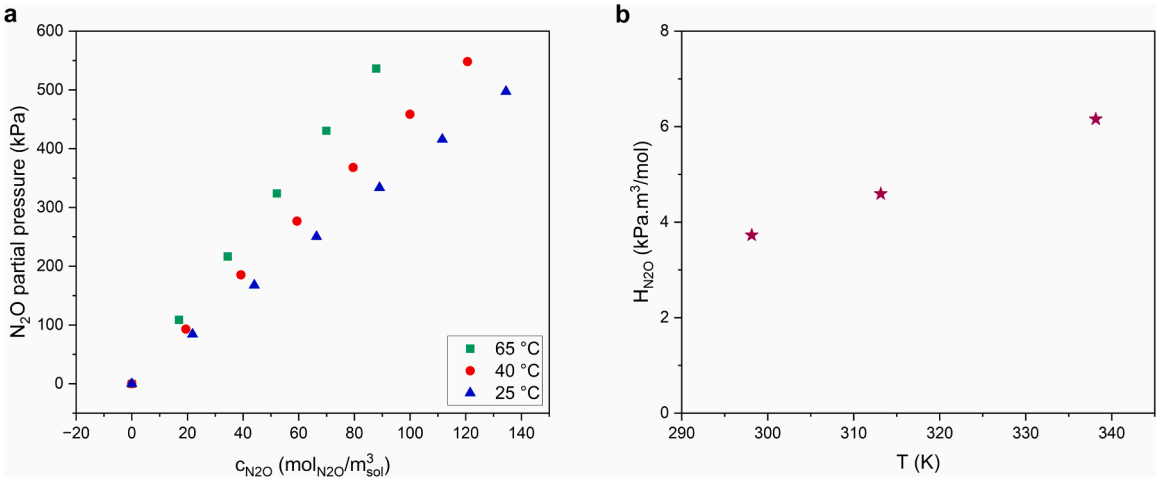

Fig. 4. Physical solubility of N_2O in 0.5 M MEA in ChCl:EG (1:4 mol ratio) as a function of temperature: (a) partial pressure of N_2O (kPa) vs. N_2O concentration (mol N_2O/m^3 sol); (b) corresponding Henry's constant. Results represent the average of duplicate measurements, with an uncertainty of less than 1%.

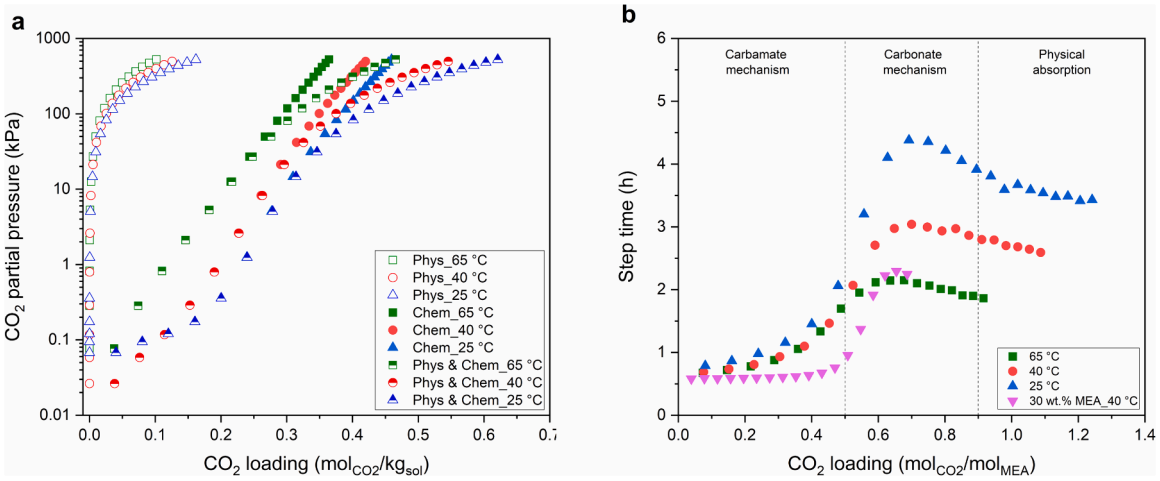

Fig. 5. (a) Equilibrium CO_2 partial pressure vs. CO_2 capacity (mol CO_2/kg sol) for 0.5 M MEA in ChCl:EG (1:4 mol ratio) at 65 °C (green), 40 °C (red), and 25 °C (blue); (b) Step time vs. CO_2 loading for 0.5 M MEA in ChCl:EG (1:4 mol ratio) at 65 °C (red), 40 °C (blue), and 25 °C (green) and 30 wt.% aqueous MEA at 40 °C (purple).

room temperature. A new absorption band appeared near 1577 cm^{-1}, corresponding to the $C = O$ stretching vibration of carbamate species (NH_2COO^-), confirming the formation of a covalent MEA-CO_2 adduct [44,45]. The increasing intensity of this band with higher MEA concentration indicates concentration-dependent CO_2 absorption behavior.

Additional bands appeared at around 1520, and 1643 cm^{-1} were attributed to the symmetric and asymmetric vibrations of $MEAH^+$ assigned to protonated MEA [46]. Furthermore, C-N and C-O stretching vibrations at 1310 and 1066 cm^{-1}, respectively, were also assigned to these species [44,46].

Collectively, these spectral features confirm that our solvent containing 0.5 M MEA in ChCl:EG (1:4) effectively facilitates carbamate formation upon CO_2 absorption, demonstrating that chemical CO_2 capture through MEA-CO_2 interactions remains active in the non-aqueous environment.

As discussed in the Introduction, carbamate stabilization is favored in the solvent environments where co-solvents with dielectric constants greater than 23 act as effective diluents for MEA [16]. EG has a dielectric constant of 37.7 at 25 °C [10]. Although experimental data for the dielectric constant of ChCl-EG mixtures are limited, the dielectric constant of the mixture is generally expected to be slightly lower than that of pure EG due to the presence of the ionic component and the formation of an extended hydrogen-bonding network [47,48]. Recent studies indicate that the dielectric response in this solvent system is primarily governed by the orientational dynamics of the hydrogen-bond donor, namely EG [48]. Therefore, in the present solvent with a ChCl:EG mol ratio of 1:4, the dielectric constant is expected to remain close to that of EG and within the range where carbamate species can be effectively stabilized. This moderate dielectric constant, lower than that of water ($\varepsilon \approx 80$ at 25 °C) but comparable to EG, supports the stabilization of ionic intermediates such as carbamate at low CO_2 partial pressures while maintaining substantial hydrogen-bond structuring and ion pairing in the solvent. Consequently, this dielectric environment provides suitable conditions for stabilizing carbamate species and supports CO_2 capture in the MEA-ChCl-EG solvent.

Interestingly, the FTIR spectra show no characteristic bicarbonate band near 1360 cm^{-1} [44,45], which is clearly evident in CO_2-loaded aqueous MEA and aqueous $KHCO_3$ reference spectra (Figure S5d). This observation confirms that bicarbonate formation does not occur in the non-aqueous MEA solvent, due to the limited water content. Instead, a new band appears at 1295 cm^{-1}, which is absent in the unloaded CO_2 sample and emerges only after CO_2 absorption. The appearance of this band exclusively under CO_2-loaded conditions indicates the formation of a new CO_2-derived species in the EG-based solvent than conventional

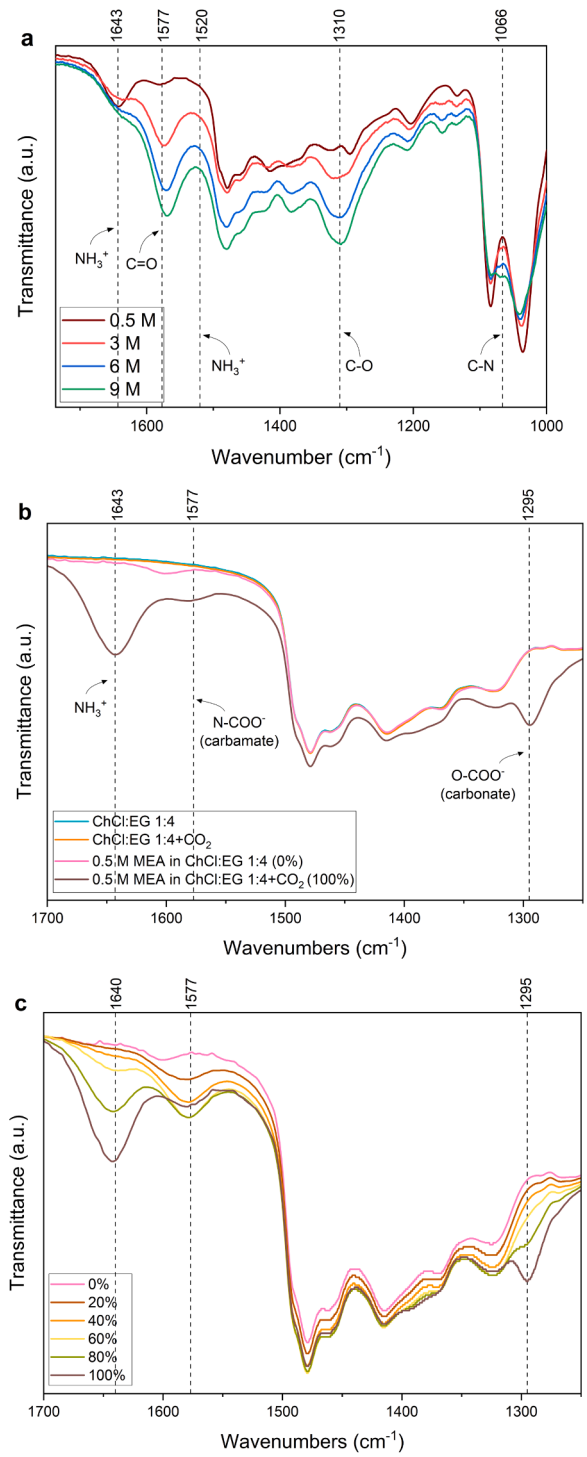

Fig. 6. FTIR Spectra of (a) MEA in ChCl:EG (1:4 mol ratio) at various MEA concentrations (0.5 M, 3 M, and 9 M) after CO_2 loading; (b) ChCl:EG (1:4 mol ratio) with and without MEA and CO_2; (c) 0.5 M MEA in ChCl:EG (1:4 mol ratio) with different CO_2 loadings (0–100%). All samples were equilibrated at ambient condition.

carbamate or bicarbonate species.

Consistent with the VLE data (Fig. 3) and FTIR results (Fig. 6b), CO_2 initially reacts predominantly with MEA to form carbamate and protonated MEA. Once the available MEA sites become saturated, additional CO_2 uptake occurs through alternative reaction pathways, where excess CO_2 interacts with the hydroxyl groups of EG, leading to the formation of carbonate-type species [49].

Although CO_2 is generally weakly reactive toward alcohols such as EG under mild conditions [49], the low-water content and basic environment created by MEA and its reaction products promotes partial deprotonation of EG, forming an alkoxide intermediate and subsequently attacks CO_2, forming the mono(2-hydroxyethyl) carbonate anion ($HOCH_2CH_2O\text{-}COO^-$) [23,38,46–50]. This carbonate formation pathway is typically reversible and governed by equilibrium limitations [49,50,53]. The proposed mechanism is consistent with previous literature, where complementary NMR-FTIR analyses have identified carbonate-related bands near 1295 cm^{-1} in glycol-based solvents [47–49].

It is important to note that this reactivity is associated specifically with the hydroxyl groups of EG rather than the hydroxyl group present in ChCl. In EG, the hydroxyl groups are neutral and can act as nucleophilic oxygen donors and, under appropriate conditions discussed above, participate in nucleophilic interactions with CO_2, enabling reversible carbonate formation [54].

In contrast, the hydroxyl group in the choline cation is strongly influenced by the adjacent quaternary ammonium center. The permanent positive charge of this ammonium group exerts a strong electron-withdrawing inductive effect, significantly reducing the electron density on the oxygen atom and thereby lowering its nucleophilicity. Furthermore, strong ionic interactions between the choline cation and chloride anion stabilize the molecular structure and limit the accessibility of the hydroxyl group for direct reaction with CO_2 [55,56]. Consequently, carbonate formation in MEA-ChCl-EG solvent is primarily associated with the hydroxyl groups of EG rather than those in ChCl.

To further investigate the interaction between EG and CO_2, additional FTIR measurements were performed on samples with different CO_2 loadings (0–100%). As previously explained, to mimic the loadings corresponding to different CO_2 partial pressures, a fully CO_2-loaded solution was first prepared by equilibrating the solvent with CO_2 at 1 bar and room temperature. This saturated solution was then serially diluted with unloaded solvent to obtain samples representing 0%, 20%, 40%, 60%, and 80% CO_2 loading.

Carbamate and carbonate species were assumed to exist in equilibrium, with their relative concentrations governed by the overall CO_2 partial pressure. As shown in Fig. 3, at a CO_2 partial pressure of 1 bar and 25 °C (marked by the red dashed line), the solvent reached a CO_2 loading of approximately 0.8 mol CO_2/mol MEA, at which carbonate formation becomes significant. When the solution is diluted to 80% loading, the equilibrium shifts back toward carbamate species.

This trend is reflected in the FTIR spectra (Fig. 6c). The carbonate band near 1295 cm^{-1} appears prominently at 80% and 100% CO_2 loadings, whereas the carbamate band at 1577 cm^{-1} is present across all loadings (20% to 100%), indicating partial conversion of carbamate to carbonate species at higher loadings. Notably, the peak intensity for 60% and 80% loadings overlaps, while the intensity decreases at 100%, suggesting that a substantial fraction of carbamate species converts to carbonate at full loading. Meanwhile, the band near 1640 cm^{-1}, assigned to protonated MEA species, increases progressively with CO_2 loading, reaching its maximum intensity at 100%.

Several studies support this mechanism. Chen et al. [52] observed a similar band at 1295 cm^{-1} by FTIR in solvents containing choline prolinate and EG after CO_2 absorption. They further confirmed by using ^{13}C NMR that this band corresponds to an EG-derived carbonate species formed through the reaction between CO_2 and the hydroxyl group of EG at CO_2 loadings above 0.5 ($\alpha > 0.5$). At lower loadings, CO_2 primarily reacts with the amino group of prolinate, while the hydroxyl group becomes reactive only after the amine sites are saturated.

Similarly, Cui et al. [51] reported two additional FTIR stretching bands at 1273 and 1394 cm^{-1} in a solvent containing IL and EG. They attributed these bands to the stretching vibration of the C=O bond in the carbonate anion, which is consistent with our observations. However, their ^{13}C NMR results further indicated that CO_2 did not directly interact with the azolide anions to form a carbamate species; instead, it only

reacted with the -OH group of EG to produce a carbonate species. Under these conditions, their proposed solvent achieved a CO_2 capture capacity of 0.118 g CO_2/g solvent at 25 °C and 1 atm.

Zhao et al. [39] identified two dominant reaction pathways for CO_2 absorption in the monoethanolamine hydrochloride-MEA-EG (MEAHCl-MEA-EG) solvent through ^{13}C NMR analysis. The first pathway involves carbamate esters formation via a zwitterionic reaction mechanism between the amino groups in the solution and CO_2, while the second pathway proceeds through deprotonation of EG, followed by its reaction with CO_2 to form carbonate species. These findings are consistent with our observations in the MEA-ChCl-EG solvent. Zhao et al. [39] further reported that increasing the EG content shifts the reaction toward greater carbonate formation. They also investigated CO_2 desorption, and found that solvents with higher EG content exhibited higher desorption rates, supporting their conclusion that carbonate species release CO_2 more readily than carbamates.

Moreover, Barzagli et al. [57] compared aqueous and non-aqueous 2-amino-2-methyl-1-propanol (AMP) based absorbents in EG-1-propanol mixtures. They demonstrated that CO_2 absorption in non-aqueous solvents follows a different pathway than in aqueous solvents. In these solvents, bicarbonate formation is suppressed, and excess CO_2 reacts with hydroxyl groups of alcohols, to form alkyl carbonates, as confirmed by ^{13}C NMR.

Therefore, in our solvent, secondary products such as carbonate species derived from EG are formed at CO_2 loading above 0.5 ($\alpha > 0.5$). This secondary pathway proceeds more slowly than the amine pathway because alcohols are weaker nucleophiles than amines [49], explaining the slower equilibration observed in the VLE experiments at high CO_2 loadings (Fig. 5b).

From a mechanistic perspective, as illustrated in Fig. 7, the enhanced CO_2 uptake in our proposed solvents results from three main contributions: (i) carbamate formation through MEA ($\alpha < 0.5$), (ii) carbonate species formation from EG at higher CO_2 partial pressures and loadings ($\alpha < 0.5$), and (iii) additional physical absorption in the non-aqueous medium. These three contributions are also schematically illustrated in Fig. 5b; however, the boundaries between the regions are not sharp and serve only to qualitatively indicate the dominant mechanisms in each loading region.

Despite the high absorption capacity of our proposed solvent, the equilibration process is noticeably slower than 30 wt.% aqueous MEA (Fig. 5b). At 40 °C, 30 wt.% aqueous MEA reaches its theoretical equilibrium capacity (~ 0.5 mol CO_2/mol MEA) within approximately 1 h, whereas our solvent requires nearly twice that time, up to 2 h to reach a similar loading at the same temperature. This slower behavior is likely attributed to two reasons. First, the formation of carbonate species through the reaction between CO_2 and EG has slower intrinsic reaction kinetics than the amine-based carbamate pathway [49]. Second, CO_2 absorption increases the viscosity of the solvent, which can introduce mass-transfer restrictions.

Overall, the ChCl-EG medium not only serves as a physical solvent but also modifies the chemical absorption pathway by enabling additional carbonate formation, thereby enhancing the total CO_2 uptake beyond the conventional carbamate-limited capacity. Nevertheless, the mass transfer limitations, likely associated with the relatively high viscosity of the solvent, represent an important factor which is discussed in the following section.

3.3. Impact of CO_2 loading and temperature on physical transport properties

3.3.1. Viscosity

Viscosity is a critical property in CO_2 capture and electrochemical conversion processes because it directly influences transport and electrochemical characteristics such as electrical conductivity, charge transfer rate, diffusion coefficient, and current density [24]. Both CO_2 absorption and temperature variations significantly affect viscosity. To investigate these effects, the viscosities of ChCl:EG solvents, with and without MEA and under CO_2 loading condition, were measured over the temperature range of 20–50 °C (Figure S6).

As expected, viscosity decreased with increasing temperature for all solvents, consistent with the typical behavior of liquids where thermal agitation reduces intermolecular interactions. Among the ChCl:EG mixtures, the 1:2 mol ratio exhibited the highest viscosity, while the 1:4 mol ratio showed the lowest. This trend suggests that increasing EG content reduces viscosity by weakening the hydrogen-bonding network and enhancing molecular mobility [58].

The neat ChCl:EG (1:4) mixture displayed slightly higher or comparable viscosity values relative to MEA-containing mixtures at 0.5 M and 3 M across the entire temperature range (Figure S6). This similarity indicates that low MEA concentrations disrupt the extensive hydrogen-bonding network in ChCl:EG, creating a more fluid structure. However, at higher MEA concentrations (6 M and 9 M), viscosity increased significantly. Introducing CO_2 into the MEA-ChCl:EG (1:4) solvent further raised viscosity, likely due to the formation of carbamate and protonated MEA, which increase structural complexity and intermolecular interactions.

Similar behavior was reported by Kazarina et al. [58] for MEA-EG mixtures. In their study, viscosity changed slightly from 9.8 mPa·s (pure MEA) to 9.6 mPa·s (pure EG) at 40 °C. However, adding ChCl (mol fraction 0.111) significantly increased viscosity to 17.5 mPa·s in MEA-rich mixtures, though it decreased to 11.8 mPa·s as EG content increased [58]. They noted that the strength of hydrogen bonds between MEA and EG differs from those in the pure components (MEA-MEA and EG-EG). However, the stronger effect of ChCl on viscosity in MEA-EG

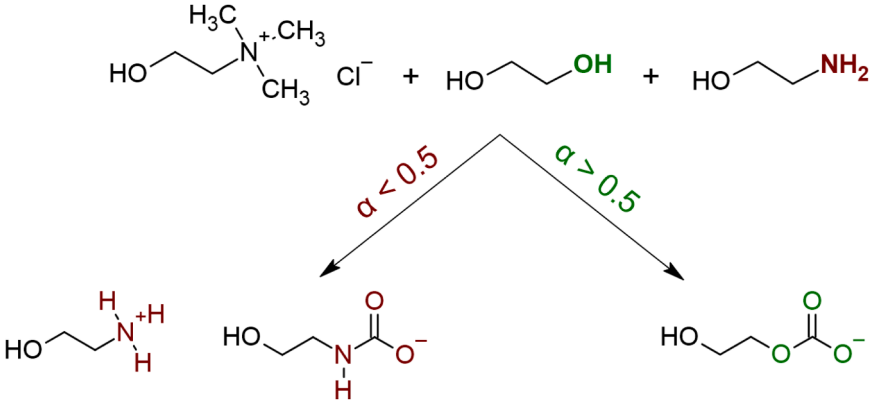

Fig. 7. Proposed chemical mechanism of CO_2 capture in 0.5 M MEA in ChCl:EG (1:4 mol ratio) solvent. At high CO_2 loadings, formation of the EG-CO_2 adduct occurs, while MEA-CO_2 adducts remain present in the solvent.

solutions indicates the new interactions dominate over hydrogen bonding. Additionally, CO_2 loading further increased viscosity compared to samples before CO_2 absorption, with the effect more pronounced at higher MEA concentrations, regardless of whether binary or ternary mixtures were considered.

The viscosity of our proposed non-aqueous MEA (0.5 M MEA in ChCl:EG 1:4) solvents is also compared to the 30 wt.% aqueous MEA in Table 1. The viscosity of the non-aqueous MEA is significantly higher than that of aqueous MEA across all temperatures, and this difference becomes more pronounced upon CO_2 loading. At 25 °C, the non-aqueous solvent exhibits a viscosity of about 17 mPa·s, which nearly doubles to 34 mPa·s after CO_2 absorption. In contrast, 30 wt.% aqueous MEA shows much lower values, increasing only from 2.5 mPa·s to 3.9 mPa·s under the same conditions [59].

Increasing temperature reduces viscosity in both solvents; however, the non-aqueous one remains substantially more viscous even at 65 °C (≈ 5 mPa·s without CO_2), compared with aqueous MEA (≈ 1.1 mPa·s) [59]. These trends indicate that while non-aqueous solvents offer advantages in CO_2 absorption, their higher viscosity, especially after CO_2 loading, may limit mass transfer and cause slow absorption kinetics. Operating at moderately elevated temperatures can partially mitigate this effect, highlighting the importance of temperature control in practical applications. Additional strategies such as compositional tuning or controlled water addition could also further reduce viscosity and improve transport properties.

3.3.2. Electrical conductivity

Electrical conductivity is another key parameter for CO_2 electrochemical conversion because low conductivity can limit current and reduce system efficiency in the integrated capture and electrochemical conversion process [24]. Electrical conductivity measurements for ChCl:EG solvents (with and without MEA and CO_2) at room temperature are shown in Table 2 and Figure S7.

A clear inverse relationship between viscosity and conductivity is observed when comparing Figures S6 and S7. Among the tested solvents, ChCl:EG (1:4 mol ratio) exhibited the highest conductivity, consistent with its low viscosity and enhanced ion mobility. The addition of MEA, followed by CO_2 absorption, progressively reduced conductivity due to increased viscosity and the formation of bulkier ionic species that hinder charge transport.

The conductivity of 0.5 M MEA in ChCl:EG (1:4 mol ratio) was 8.5 mS/cm at room temperature, significantly higher than 30 wt.% aqueous MEA (0.7 mS/cm at 20 °C) [60]. This difference arises because ChCl provides inherently mobile ionic species (Ch^+ and Cl^-), while MEA dissolved in water generates only limited charge carriers ($MEAH^+$ and OH^-).

The neat ChCl:EG has conductivity of 9.1 mS/cm at room temperature [35] and 9.5 mS/cm at 40 °C [61]. Introducing 0.5 M MEA slightly reduced conductivity to 8.5 mS/cm, and full CO_2 loading further decreased it to 6.5 mS/cm. In contrast, CO_2-loaded 30 wt.% aqueous MEA showed a substantial conductivity increase to 11.75–27.40 mS/cm (depending on α in the range of 0.15–0.50) at 20 °C [60], primarily due to the formation of mobile carbamate and bicarbonate species in its low-viscosity environment.

Han et al. [62] also reported that in aqueous MEA, conductivity increases with MEA concentration up to 2 M but declines beyond this point due to limited water for ion solvation. A similar trend was observed in our solvent, where conductivity decreased with higher MEA concentrations, primarily due to increased viscosity rather than ion-pair formation (Figure S7).

Table 1
Comparison of viscosity (mPa.s) of non-aqueous and aqueous MEA solvents under CO_2-Free and CO_2-equilibrated conditions (at 1 bar and room temperature) at different temperatures.

T (°C)	0.5 M MEA in ChCl:EG (1:4 mol ratio)		30 wt.% aqueous MEA [59]	
	CO_2-free	CO_2-equilibrated	CO_2-free	CO_2-equilibrated
25	17	34	2.5	3.9
40	10	18	1.7	2.7
65	5	7	1.1	1.8

Table 2
Comparison of electrical conductivity (mS/cm) of non-aqueous and aqueous MEA solvents under CO_2-Free and CO_2-equilibrated conditions (at 1 bar and room temperature) at room temperature.

Sample name	CO_2-free	CO_2-equilibrated
ChCl:EG (1:4 mol ratio)	9.1	-
0.5 M MEA in ChCl:EG (1:4 mol ratio)	8.5	6.5
30 wt.% aqueous MEA at 20 °C [60]	0.7	27.4

For our proposed integrated CO_2 capture and electrochemical conversion process, the use of non-aqueous MEA-ChCl-EG solvent offers several advantages. In particular, the incorporation of ChCl introduces stable ionic charge carriers (Ch^+ and Cl^-) that enhance electrolyte conductivity. Consequently, electrical conductivity in this non-aqueous solvent is largely independent of CO_2 speciation. This contrasts with aqueous MEA solvents, where conductivity strongly depends on the concentration of carbamate and protonated MEA species, both of which are temperature dependent.

This distinction becomes particularly important under elevated operating temperatures relevant for our integrated electrochemical conversion process (around 65 °C) [43]. In aqueous electrolytes, increasing temperature shifts equilibrium toward CO_2 desorption, reducing the concentration of mobile ionic species and thereby lowering conductivity. In contrast, the MEA-ChCl-EG solvent maintains stable ionic species, while the increase in temperature reduces viscosity and enhances ion mobility, resulting in improved electrical conductivity.

Despite these advantages, the relatively high viscosity of our non-aqueous solvent introduces an important limitation. Elevated viscosity restricts CO_2 diffusion and interfacial mass transport to the electrode surface, as observed in our previous work [43], thereby constraining the overall CO_2 conversion rate in electrochemical conversion process. Although the enhanced electrical conductivity provided by ChCl partially compensates for ohmic losses, it cannot fully offset for the transport limitations imposed by viscosity. Consequently, the overall solvent performance reflects a trade-off between electrical conductivity and mass-transfer efficiency.

Nevertheless, the ChCl:EG (1:4 mol ratio) solvent containing 0.5 M MEA represents a promising compromise, providing sufficient electrical conductivity while maintaining manageable viscosity. These results highlight that viscosity control, alongside electrical conductivity, remains a critical parameter for further solvent optimization. Future strategies such as compositional tuning, controlled water addition, or temperature optimization will be therefore essential to reduce viscosity while preserving conductivity, stability, and electrochemical performance in integrated CO_2 capture and electrochemical conversion processes.

3.4. Thermal stability

MEA degradation during CO_2 capture primarily occurs through oxidative or thermal degradation pathways [63]. Oxidative degradation occurs in the presence of oxygen at elevated temperature, typically in coal-fired power plant flue gas and leads to MEA breakdown during the absorption stage [64]. Thermal degradation, on the other hand, takes place in the presence of CO_2 at elevated temperatures such as those encountered in the stripper. Thermal stability is therefore a critical property for solvents used in capture-conversion processes, as it determines the maximum operating temperature at which the solvent can function without significant mass loss or degradation [63].

In this study, we focused only on thermal stability because the

operating temperature in our integrated capture-conversion process is designed to remain below 80 °C [43]. No further investigation was conducted on the specific degradation products or the underlying chemistry. TGA was performed to evaluate the thermal decomposition temperature of ChCl:EG-based solvents, with and without MEA and CO_2, over the temperature range of 20–160 °C (Fig. 8). This analysis also allows assessment of how ChCl and EG influence the thermal stability of MEA under these conditions compared with 30 wt.% aqueous MEA.

The results show that the pure components exhibited distinct thermal behaviors. MEA and EG showed the highest volatility, with rapid and substantial mass loss near their respective boiling points (170 °C for MEA and 197.3 °C for EG) [10,18]. The onset decomposition temperature for EG has been reported at approximately 240 °C [10], although this value can vary depending on heating rate, sample mass, and atmosphere. In contrast, ChCl remained thermally stable with negligible mass loss within the investigated temperature range, consistent with its non-volatile salt nature and high decomposition temperature (>302 °C) [65].

The ChCl:EG (1:4 mol ratio) mixture significantly reduced the volatility of EG, resulting in substantially lower mass loss compared with pure EG, consistent with observations reported by Ruan et al. [38]. The addition of 0.5 M MEA slightly increased volatility; however, the mixture remained considerably more stable than the individual components MEA or EG, in agreement with observations by Kazarina et al. [58]. Upon CO_2 absorption, MEA-containing mixtures exhibited moderate increases in mass loss, likely due to partial disruption of the hydrogen-bonding network and, importantly, as the reaction equilibrium (Reaction 3) shifts back toward CO_2 desorption at elevated temperatures.

Comparing our results with literature reports, Ma et al. [66] observed that 30 wt.% aqueous MEA begins thermal decomposition at 70 °C. Kang et al. [67] further assessed the thermal stability of MEA-based solvents using TGA for three solvents, aqueous MEA (MEA/H_2O), quasi-aqueous MEA (MEA/H_2O/EG), and non-aqueous MEA (MEA/EG). Their results showed that aqueous MEA remained stable up to 100 °C, whereas the addition of EG significantly improved thermal stability, with the quasi-aqueous mixture stable up to 130 °C and the non-aqueous MEA/EG solvent reaching 140 °C. These findings demonstrate that reducing water content and incorporating EG as a co-solvent markedly improve thermal stability, while reducing volatility and degradation at elevated temperatures.

Moreover, Lee et al. [50] reported that upon addition of CO_2 to a mixture containing ILs and EG, a carbonate species is formed through reaction with EG. The charged species in the IL interact electrostatically with the carbonate anion via coulombic interactions. These interactions stabilize the carbonate complex, reducing its volatility and preventing solvent loss during regeneration.

Our present results align with this behavior, indicating that ChCl acts as a stabilizing agent, making MEA-EG based solvents more suitable for high-temperature CO_2 capture and electrochemical conversion processes.

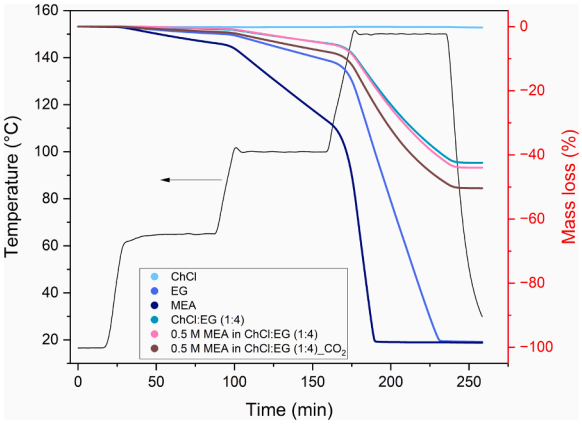

Fig. 8. Thermal stability of ChCl, EG, MEA and ChCl:EG (1:4 mol ratio), and 0.5 M MEA in ChCl:EG (1:4 mol ratio) in both fully CO_2-loaded and unloaded conditions. Measurements were conducted over a temperature range of 25–150 °C at a heating rate of 3 °C/min under an argon atmosphere. Temperature and mass loss (%) are plotted as functions of time. The black curve represents the temperature profile as a function of time, while the remaining curves show mass loss (%) as a function of temperature.

3.5. Heat of absorption

After confirming the CO_2 absorption performance of our solvent, the next step is to evaluate its energy requirements for the integrated capture-conversion process. Among the relevant parameters, the heat of absorption is particularly important because it largely determines the energy required for solvent regeneration.

In our integrated process, CO_2 is desorbed in-situ within the electrolyzer at an elevated temperature (65 °C), where it is simultaneously reduced to CO. To estimate the energy required for CO_2 release, the total heat demand (Q_{tot}) can be expressed as [57,68]:

$$Q_{tot} = Q_{sens} + Q_{vap} + \Delta Q_{des} \quad (7)$$

where Q_{sens} is the sensible heat to raise the solution temperature from absorption to desorption temperature, Q_{vap} is the heat needed to vaporize the solution in the regenerator column, and ΔQ_{des} (approximately equal to absolute value of ΔH_{abs}) is the heat of CO_2 desorption, which is the great portion of the total regeneration heat (approximately 50–60%) [68].

In this study, ΔH_{abs} was estimated using the Clausius-Clapeyron equation rather than measured directly by calorimetry technique. The purpose of this calculation was to provide a qualitative indication of changes in absorption behavior and observe possible shifts in reaction mechanisms. It is important to recognize that this approach relies on several simplifying assumptions, and careful interpretation of the associated VLE data is therefore required [69]. During the VLE measurements, the following assumptions were applied: (i) the vapor pressure of the solvent is not changing upon CO_2 absorption; (ii) equilibrium is achieved at a certain point; and (iii) the pressure transducer operates with high precision. Additional assumptions inherent to the Clausius-Clapeyron approach include ideal gas behavior of the vapor phase, negligible liquid-phase molar volume, and a temperature-independent enthalpy of vaporization [13,69]. Because to these simplifications, the calculated ΔH_{abs} values should be interpreted as indicative trends rather than absolute thermodynamic quantities measured by calorimetric technique, which are typically more accurate and measured at certain isothermal conditions [11,70].

The calculated ΔH_{abs} for 0.5 M MEA in ChCl:EG (1:4 mol ratio), together with associated uncertainties, are presented in Table S5 and Figure S10. The relatively large error bars primarily result from the propagation of uncertainties associated with VLE measurements, pressure determination, temperature control, and regression analysis applied in the Clausius-Clapeyron calculation. A detailed description of the uncertainty analysis and error propagation methodology is provided in the Supporting Information.

Using this approach, $|\Delta H_{abs}|$ for our proposed solvent was estimated to be approximately 66 kJ/mol at low CO_2 loadings ($\alpha < 0.5$ mol CO_2/mol MEA). As the CO_2 loading increased, $|\Delta H_{abs}|$ decreased substantially to around 22 kJ/mol (Figure S10). As previously discussed, at low CO_2 partial pressures , CO_2 absorption is dominated by carbamate formation, a significant contributor to the heat of absorption due to the strong chemical bonding and high reaction enthalpy [71]. At higher CO_2 partial pressures , however, the formation of EG carbonate species and physical absorption become more dominant, both of which require less energy [71]. These results therefore provide qualitative evidence for the

shift in absorption mechanism identified in the spectroscopic analysis.

For comparison, the calorimetrically measured $|\Delta H_{abs}|$ of 30 wt.% aqueous MEA at $\alpha \sim 0.5$ mol CO_2/mol MEA is approximately 84 kJ/mol at 40 °C [68,71]. The higher heat of absorption in the aqueous solvents primarily arises from carbamate formation and high specific heat capacity of water (4.184 kJ/kg.K at 25 °C) [72] and its significant vaporization enthalpy, resulting in a substantial energy penalty.

Interestingly, Wanderley et al. [11] reported that the calorimetrically measured heats of absorption for 30 wt.% aqueous MEA and 30 wt.% MEA dissolved in pure EG at 40 °C were nearly similar. However, their study also highlighted that the low volatility of EG-containing solvents could significantly reduce overall reboiler heat duty compared with conventional aqueous MEA solvents. In addition, EG has a significantly lower specific heat capacity (2.4 kJ/kgK at 25 °C) [12,72], meaning that replacing water with a non-aqueous co-solvent such as ChCl:EG effectively can reduce the energy consumption required for solvent regeneration, providing a potentially more energy-efficient alternative for CO_2 capture.

4. Conclusion

This study presented a comprehensive evaluation of a non-aqueous solvent consisting of 0.5 M MEA in ChCl:EG (1:4 mol ratio) as a single medium for integrated CO_2 capture and electrochemical conversion. The VLE measurements, spectroscopic analysis, and physical transport properties of the solvent were evaluated to assess its suitability for such processes.

VLE measurements demonstrated that, while conventional 30 wt.% aqueous MEA exhibits stronger CO_2 binding at low partial pressures ($\leq$1 kPa), our non-aqueous MEA solvent achieves substantially higher CO_2 capacities at moderate to high pressures (up to 500 kPa), reaching up to 1.2, 1.1, and 0.9 mol CO_2/mol MEA at 25, 40, and 65 °C, respectively, exceeding the theoretical equilibrium limit of aqueous MEA. Complementary N_2O solubility measurements enabled separation of physical and chemical absorption contributions, showing that chemical absorption dominates while physical solubility also contributes to the overall uptake.

FTIR analysis further revealed that the enhanced CO_2 capacity originates from two reaction mechanisms, a transition from carbamate formation at low CO_2 partial pressures to increased carbonate formation and physical absorption at higher CO_2 partial pressures.

Although incorporation of ChCl increased solvent viscosity due to its bulkier ionic structure, it significantly enhanced the thermal stability of MEA and EG and provided ionic conductivity, resulting in improved electrical conductivity required for electrochemical operation. Despite the higher viscosity, especially after CO_2 loading, which may hinder mass transfer and slow absorption kinetics, the low volatility of the ChCl:EG co-solvent further reduces solvent loss and impacts lowering regeneration energy demand.

Overall, the MEA-ChCl-EG solvent shows potential for integrated CO_2 capture and electrochemical conversion, offering high CO_2 absorption capacity, sufficient electrical conductivity, and improved thermal stability. Although the relatively high viscosity may limit mass transfer, strategies such as temperature optimization, compositional tuning, or controlled water addition could improve transport properties while preserving the advantages of the non-aqueous solvent. These findings provide insights for designing non-aqueous solvents for integrated CCU technologies.

Appendix A. Supporting Information

Additional experimental details and methods are available in supporting information document, including detailed results for VLE measurements, FTIR, viscosity, electrical conductivity, density, thermal stability, and heat of absorption.

Funding sources declaration

TOeLS, a programme co-financed by Shell and a PPP-allowance from Top Consortia for Knowledge and Innovation (TKI's) of the Ministry of Economic Affairs and Climate in the context of the TU Delft e-Refinery program, the Netherlands.

CRediT authorship contribution statement

Hengameh Farahmandazad: Writing – review & editing, Writing – original draft, Visualization, Validation, Software, Methodology, Investigation, Formal analysis, Data curation, Conceptualization. **Nishant Sharma:** Writing – review & editing, Methodology, Formal analysis, Data curation. **Iris Burgers:** Writing – review & editing, Methodology, Formal analysis, Data curation. **Earl Goetheer:** Writing – review & editing, Supervision, Methodology, Investigation, Conceptualization. **Wiebren de Jong:** Writing – review & editing, Supervision, Resources, Project administration, Methodology, Investigation, Funding acquisition, Conceptualization.

Declaration of competing interest

The authors declare that they have no known competing financial interests or personal relationships that could have appeared to influence the work reported in this paper.

Acknowledgments

The authors would like to acknowledge the funding from TOeLS, a programme co-financed by Shell and a PPP-allowance from Top Consortia for Knowledge and Innovation (TKI's) of the Ministry of Economic Affairs and Climate in the context of the TU Delft e-Refinery program.

The authors acknowledge TNO for conducting the VLE measurements. The authors would also thank Michel van den Brink for his laboratory support and Hans Brouwer for performing the TGA measurements.

Supplementary materials

Supplementary material associated with this article can be found, in the online version, at doi:10.1016/j.ceja.2026.101143.

Data availability

No data was used for the research described in the article.

References

[1] R. Socolow, M. Desmond, R. Aines, J. Blackstock, O. Bolland, T. Kaarsberg, N. Lewis, M. Mazzotti, A. Pfeffer, K. Sawyer, J. Siirola, B. Smit, J. Wilcox, Direct air capture of CO_2 with Chemicals Panel on Public Affairs, Am. Phys. Soc. - Panel Public Aff. (2011) 100.

[2] Global Monitoring Laboratory, *Monthly average Mauna Loa* CO_2, accessed, https://www.esrl.noaa.gov/gmd/ccgg/trends/, 2026. accessed-01-08.

[3] UNFCC. United Nations Framework Convention on Climate Change - the Paris Agreement. 2015.

[4] S.E. Jerng, B.M. Gallant, Electrochemical reduction of CO_2 in the captured State using aqueous or nonaqueous amines, iScience 25 (7) (2022) 104558, https://doi.org/10.1016/j.isci.2022.104558.

[5] C. Chao, Y. Deng, R. Dewil, J. Baeyens, X. Fan, Post-combustion carbon capture, Renew. Sustain. Energy Rev. 138 (2021) 110490, https://doi.org/10.1016/j.rser.2020.110490.

[6] X. Wang, C. Song, Carbon capture from flue gas and the atmosphere: a perspective, Front. Energy Res. 8 (2020), https://doi.org/10.3389/fenrg.2020.560849.

[7] T. N.Borhani, M. Wang, Role of solvents in CO_2 capture processes: the review of selection and design methods, Renew. Sustain. Energy Rev. 114 (2019) 109299, https://doi.org/10.1016/j.rser.2019.109299.

[8] I. Sullivan, A. Goryachev, I.A. Digdaya, X. Li, H.A. Atwater, D.A. Vermaas, C. Xiang, Coupling electrochemical CO_2 conversion with CO_2 capture, Nat. Catal. 4 (11) (2021) 952–958, https://doi.org/10.1038/s41929-021-00699-7.

[9] H.M. Pelzer, N. Kolobov, D.A. Vermaas, T. Burdyny, Scaling and heating will drive low-temperature CO_2 electrolysers to operate at higher temperatures, Nat. Energy 10 (2025) 549–556, https://doi.org/10.1038/s41560-025-01745-5.

[10] The MEGlobal Group of Companies, *Ethylene glycol product* guide. https://www.magnumsolvent.com/productdata/Product, 2005. Literature/Heat Transfer Fluids/Product guide - Ethylene Glycol.pdf.

[11] R.R. Wanderley, D.D.D. Pinto, H.K. Knuutila, Investigating opportunities for water-lean solvents in CO_2 capture: VLE and heat of absorption in water-lean solvents containing MEA, Sep. Purif. Technol. 231 (2020) 115883, https://doi.org/10.1016/j.seppur.2019.115883.

[12] H. Guo, C. Li, X. Shi, H. Li, S. Shen, Nonaqueous amine-based absorbents for energy efficient CO_2 capture, Appl. Energy 239 (2019) 725–734, https://doi.org/10.1016/j.apenergy.2019.02.019.

[13] H.S. Salehi, Molecular Simulation of Deep Eutectic Solvents (Dissertation), Delft University of Technology, 2022, https://doi.org/10.4233/uuid:a802da95-9c59-41a3-ab87-9ad2d7d4b25f.

[14] H.S. Salehi, M. Ramdin, O.A. Moultos, T.J.H. Vlugt, Computing solubility parameters of deep eutectic solvents from molecular dynamics simulations, Fluid Phase Equilib. 497 (2019) 10–18, https://doi.org/10.1016/j.fluid.2019.05.022.

[15] B. Gwinner, D. Roizard, F. Lapicque, E. Favre, R. Cadours, P. Boucot, P.-L. Carrette, CO_2 capture in flue gas: semiempirical approach to select a potential physical solvent, Ind. Eng. Chem. Res. 45 (14) (2006) 5044–5049, https://doi.org/10.1021/ie0580396.

[16] I.L. Leites, Thermodynamics of CO_2 solubility in mixtures monoethanolamine with organic solvents and water and commercial experience of energy saving gas purification technology, Energy Convers. Manag. 39 (16) (1998) 1665–1674, https://doi.org/10.1016/S0196-8904(98)00076-4.

[17] G. Akerlof, Dielectric constants of some organic solvent-water mixtures at various temperatures, J. Am. Chem. Soc. 54 (11) (1932) 4125–4139, https://doi.org/10.1021/ja01350a001.

[18] D.R. Lide, CRC Handbook of Chemistry and Physics, CRC press, 2005.

[19] W. Zeng, Y. Du, Y. Xue, H.L Frisch, in: J.E. Mark (Ed.), Solubility Parameters BT - Physical Properties of Polymers Handbook, Springer New York, New York, NY, 2007, pp. 289–303, https://doi.org/10.1007/978-0-387-69002-5_16.

[20] V.L. Martins, R.M. Torresi, Ionic liquids in electrochemical energy storage, Curr. Opin. Electrochem. 9 (2018) 26–32, https://doi.org/10.1016/j.coelec.2018.03.005.

[21] C. Zhang, L. Zhang, G. Yu, Eutectic electrolytes as a promising platform for next-generation electrochemical energy storage, Acc. Chem. Res. 53 (8) (2020) 1648–1659, https://doi.org/10.1021/acs.accounts.0c00360.

[22] A. Sharma, R. Sharma, R.C. Thakur, L. Singh, An overview of deep eutectic solvents: alternative for organic electrolytes, aqueous systems & ionic liquids for electrochemical energy storage, J. Energy Chem. 82 (2023) 592–626, https://doi.org/10.1016/j.jechem.2023.03.039.

[23] I. Cichowska-Kopczyńska, B. Nowosielski, D. Warmińska, Deep eutectic solvents: properties and applications in CO_2 separation, Molecules 28 (14) (2023), https://doi.org/10.3390/molecules28145293.

[24] S. Dongare, M. Zeeshan, A.S. Aydogdu, R. Dikki, S.F. Kurtoğlu-Öztulum, O. K. Coskun, M. Muñoz, A. Banerjee, M. Gautam, R.D. Ross, Reactive capture and electrochemical conversion of CO_2 with ionic liquids and deep eutectic solvents, Chem. Soc. Rev. 53 (17) (2024) 8563–8631, https://doi.org/10.1039/D4CS00390J.

[25] E.L. Smith, A.P. Abbott, K.S. Ryder, Deep eutectic solvents (DESs) and their applications, Chem. Rev. 114 (21) (2014) 11060–11082, https://doi.org/10.1021/cr300162p.

[26] W. Wang, M.M. Sabugaa, S. Chandra, Y.P. Asmara, B. Abd Alreda, N. Ulloa, Y. Elmasry, M.M. Kadhim, Choline chloride-based deep eutectic solvents as electrolytes for wide temperature range supercapacitors, J. Energy Storage 71 (2023) 108141, https://doi.org/10.1016/j.est.2023.108141.

[27] N. Ahmad, X. Wang, P. Sun, Y. Chen, F. Rehman, J. Xu, X. Xu, Electrochemical CO_2 reduction to CO facilitated by MDEA-based deep eutectic solvent in aqueous solution, Renew. Energy 177 (2021) 23–33, https://doi.org/10.1016/j.renene.2021.05.106.

[28] D.V. Vasilyev, A.V. Rudnev, P. Broekmann, P.J Dyson, A general and facile approach for the electrochemical reduction of carbon dioxide inspired by deep eutectic solvents, ChemSusChem 12 (8) (2019) 1635–1639, https://doi.org/10.1002/cssc.201900579.

[29] M.K. AlOmar, M. Hayyan, M.A. Alsaadi, S. Akib, A. Hayyan, M.A. Hashim, Glycerol-based deep eutectic solvents: physical properties, J. Mol. Liq. 215 (2016) 98–103, https://doi.org/10.1016/j.molliq.2015.11.032.

[30] J.M. Klein, H. Squire, W. Dean, B.E. Gurkan, From salt in solution to solely ions: solvation of methyl viologen in deep eutectic solvents and ionic liquids, J. Phys. Chem. B 124 (29) (2020) 6348–6357, https://doi.org/10.1021/acs.jpcb.0c03296.

[31] R.B. Leron, M.-H. Li, Solubility of carbon dioxide in a choline chloride-ethylene glycol based deep eutectic solvent, Thermochim. Acta 551 (2013) 14–19, https://doi.org/10.1016/j.tca.2012.09.041.

[32] H. Fu, X. Wang, H. Sang, J. Liu, X. Lin, L. Zhang, Highly efficient absorption of carbon dioxide by EG-assisted DBU-based deep eutectic solvents, *J. CO_2 Util.* 43 (2021) 101372, https://doi.org/10.1016/j.jcou.2020.101372.

[33] V. Agieienko, R. Buchner, Is ethaline a deep eutectic solvent? Phys. Chem. Chem. Phys. 24 (9) (2022) 5265–5268, https://doi.org/10.1039/D2CP00104G.

[34] M.H. Oyevaar, R.W.J. Morssinkhof, K.R. Westerterp, Density, viscosity, solubility, and diffusivity of carbon dioxide and nitrous oxide in solutions of diethanolamine in aqueous ethylene glycol at 298 K, J. Chem. Eng. Data 34 (1) (1989) 77–82, https://doi.org/10.1021/je00055a022.

[35] H. Farahmandazad, S. Asperti, R. Kortlever, E. Goetheer, W. de Jong, Effect of halide anions on electrochemical CO_2 reduction in non-aqueous choline solutions using Ag and Au electrodes, ChemistryOpen 13 (11) (2024) e202400166, https://doi.org/10.1002/open.202400166.

[36] S. Garg, M. Li, T.E. Rufford, L. Ge, V. Rudolph, R. Knibbe, M. Konarova, G.G. X Wang, Catalyst-electrolyte interactions in aqueous reline solutions for highly selective electrochemical CO_2 reduction, ChemSusChem 13 (2) (2020) 304–311, https://doi.org/10.1002/cssc.201902433.

[37] S. Garg, M. Li, Y. Wu, M. Nazmi Idros, H. Wang, A.J. Yago, L. Ge, G.G.X. Wang, T. E. Rufford, Understanding the effects of anion interactions with Ag electrodes on electrochemical CO_2 reduction in choline halide electrolytes, ChemSusChem 14 (12) (2021) 2601–2611, https://doi.org/10.1002/cssc.202100848.

[38] C. Ruan, H.J. Heeres, J. Yue, 5-Hydroxymethylfurfural synthesis from fructose over deep eutectic solvents in batch reactors and continuous flow microreactors, J. Flow Chem. 13 (2) (2023) 155–168, https://doi.org/10.1007/s41981-023-00262-4.

[39] R. Zhao, Y. Zhen, C. Zhu, T. Fu, X. Gao, Y. Ma, The promotion mechanism of ethylene glycol on the absorption and desorption performance of CO_2 in ethanolamine hydrochloride based deep eutectic solvents, Chem. Eng. Sci. 306 (2025) 121298, https://doi.org/10.1016/j.ces.2025.121298.

[40] S.S. Laddha, J.M. Diaz, P.V. Danckwerts, The N_2O analogy: the solubilities of CO_2 and N_2O in aqueous solutions of organic compounds, Chem. Eng. Sci. 36 (1) (1981) 228–229, https://doi.org/10.1016/0009-2509(81)80074-7.

[41] H. Guo, X. Shi, S. Shen, Solubility of N_2O and CO_2 in non-aqueous systems of monoethanolamine and glycol ethers: measurements and model representation, J. Chem. Thermodyn. 137 (2019) 76–85, https://doi.org/10.1016/j.jct.2019.05.017.

[42] M.T. Mota-Martinez, J.P. Hallett, N. Mac Dowell, Solvent selection and design for CO_2 capture - how we might have been missing the point, Sustain. Energy Fuels 1 (10) (2017) 2078–2090, https://doi.org/10.1039/C7SE00404D.

[43] H. Farahmandazad, A. Grütter, S. Fu, R. Kortlever, E. Goetheer, W. de Jong, Enhancing electrochemical CO_2-to-CO conversion in a nonaqueous amine-based electrolyte at elevated temperature via pulsed electrolysis and EDTA, ACS Electrochem. (2025), https://doi.org/10.1021/acselectrochem.5c00197.

[44] K. Robinson, A. McCluskey, M.I. Attalla, An ATR-FTIR study on the effect of molecular structural variations on the CO_2 absorption characteristics of heterocyclic amines, part II, ChemPhysChem 13 (9) (2012) 2331–2341, https://doi.org/10.1002/cphc.201200066.

[45] C. Sun, P.K. Dutta, Infrared spectroscopic study of reaction of carbon dioxide with aqueous monoethanolamine solutions, Ind. Eng. Chem. Res. 55 (22) (2016) 6276–6283, https://doi.org/10.1021/acs.iecr.6b00017.

[46] G. Richner, G. Puxty, Assessing the chemical speciation during CO_2 absorption by aqueous amines using in situ FTIR, Ind. Eng. Chem. Res. 51 (44) (2012) 14317–14324, https://doi.org/10.1021/ie302056f.

[47] Y. Wang, C. Ma, C. Liu, X. Lu, X. Feng, X. Ji, Thermodynamic study of choline chloride-based deep eutectic solvents with water and methanol, J. Chem. Eng. Data 65 (5) (2020) 2446–2457, https://doi.org/10.1021/acs.jced.9b01113.

[48] D. Reuter, C. Binder, P. Lunkenheimer, A. Loidl, Ionic conductivity of deep eutectic solvents: the role of orientational dynamics and glassy freezing, Phys. Chem. Chem. Phys. 21 (13) (2019) 6801–6809, https://doi.org/10.1039/C9CP00742C.

[49] K. Tomishige, Y. Gu, Y. Nakagawa, M. Tamura, Reaction of CO_2 with alcohols to linear-, cyclic-, and poly-carbonates using CeO_2-based catalysts, Front. Energy Res. 8 (2020) 117, https://doi.org/10.3389/fenrg.2020.00117.

[50] Y.-Y. Lee, D. Penley, A. Klemm, W. Dean, B. Gurkan, Deep eutectic solvent formed by imidazolium cyanopyrrolide and ethylene glycol for reactive CO_2 separations, ACS Sustain. Chem. Eng. 9 (3) (2021) 1090–1098, https://doi.org/10.1021/acssuschemeng.0c07217.

[51] G. Cui, M. Lv, D. Yang, Efficient CO_2 absorption by azolide-based deep eutectic solvents, Chem. Commun. 55 (10) (2019) 1426–1429, https://doi.org/10.1039/C8CC10085C.

[52] M. Chen, J. Xu, CO_2 capture mechanism by deep eutectic solvents formed by choline prolinate and ethylene glycol, Molecules 28 (14) (2023) 5461, https://doi.org/10.3390/molecules28145461.

[53] Y. Gu, M. Tamura, Y. Nakagawa, K. Nakao, K. Suzuki, K. Tomishige, Direct synthesis of polycarbonate diols from atmospheric flow CO_2 and diols without using dehydrating agents, Green Chem. 23 (16) (2021) 5786–5796, https://doi.org/10.1039/D1GC01172C.

[54] F.L. Bleken, K.J. Jens, K.-A. Solli, O. Swang, CO_2 utilization through reaction with alcohols: a quantum chemical study, Ind. Eng. Chem. Res. 64 (46) (2025) 22084–22091, https://doi.org/10.1021/acs.iecr.5c02744.

[55] Perkins, S.L.; Painter, P.; Colina, C.M. Experimental and computational studies of choline chloride-based deep eutectic solvents. 2014. https://doi.org/10.1021/je500520h.

[56] G. García, M. Atilhan, S. Aparicio, A theoretical study on mitigation of CO_2 through advanced deep eutectic solvents, Int. J. Greenh. Gas Control. 39 (2015) 62–73, https://doi.org/10.1016/j.ijggc.2015.05.004.

[57] F. Barzagli, C. Giorgi, F. Mani, M. Peruzzini, Comparative study of CO_2 capture by aqueous and nonaqueous 2-amino-2-methyl-1-propanol based absorbents carried out by 13C NMR and enthalpy analysis, Ind. Eng. Chem. Res. 58 (11) (2019) 4364–4373, https://doi.org/10.1021/acs.iecr.9b00552.

[58] O.V. Kazarina, V.N. Agieienko, A.N. Petukhov, A.V. Vorotyntsev, A.S. Kazarin, M. E. Atlaskina, A.A. Atlaskin, A.N. Markov, A.A. Golovacheva, I.V Vorotyntsev, Monoethanolamine+ ethylene glycol+ choline chloride: an effect of the mixture composition on the CO_2 absorption capacity, density, and viscosity, J. Chem. Eng. Data 67 (10) (2022) 2899–2912, https://doi.org/10.1021/acs.jced.2c00245.

[59] T.G. Amundsen, L.E. Øi, D.A. Eimer, Density and viscosity of monoethanolamine+ water+ carbon dioxide from (25 to 80) °C, J. Chem. Eng. Data 54 (11) (2009) 3096–3100, https://doi.org/10.1021/je900188m.
[60] H. Ju, W. ElMoudir, A. Aboudheir, N. Mahinpey, Density, viscosity, refractive index, and electrical conductivity of degraded monoethanolamine solutions at standard temperatures, J. Chem. Eng. Data 63 (6) (2018) 1969–1976, https://doi.org/10.1021/acs.jced.7b01101.
[61] M. Zhong, Q.F. Tang, Y.W. Zhu, X.Y. Chen, Z.J. Zhang, An alternative electrolyte of deep eutectic solvent by choline chloride and ethylene glycol for wide temperature range supercapacitors, J. Power Sources 452 (2020) 227847, https://doi.org/10.1016/j.jpowsour.2020.227847.
[62] S.-J. Han, J.-H. Wee, Estimation of the amount of CO_2 absorbed by measuring the variation of electrical conductivity in highly concentrated monoethanolamine solvent systems, J. Chem. Eng. Data 61 (2) (2016) 712–720, https://doi.org/10.1021/acs.jced.5b00178.
[63] D. Mullen, L. Braakhuis, H.K. Knuutila, J. Gibbins, M. Lucquiaud, Monoethanolamine degradation rates in post-combustion CO_2 capture plants with the capture of 100% of the added CO_2, Ind. Eng. Chem. Res. 63 (31) (2024) 13677–13691, https://doi.org/10.1021/acs.iecr.4c01525.
[64] K.-S. Zoannou, D.J. Sapsford, A.J. Griffiths, Thermal degradation of monoethanolamine and its effect on CO_2 capture capacity, Int. J. Greenh. Gas Control 17 (2013) 423–430, https://doi.org/10.1016/j.ijggc.2013.05.026.
[65] A.L. Sazali, N. AlMasoud, S.K. Amran, T.S. Alomar, K.F. Pa'ee, Z.M. El-Bahy, T.-L. K. Yong, D.J. Dailin, L.F. Chuah, Physicochemical and thermal characteristics of choline chloride-based deep eutectic solvents, Chemosphere 338 (2023) 139485, https://doi.org/10.1016/j.chemosphere.2023.139485.
[66] L. Ma, Y. Ding, X. Zhu, H. Wang, M. Cheng, Q. Liao, M.onoethanolamine (MEA) and N,N-dimethylformamide (DMF) with fast absorption rate as nonaqueous absorbent for CO_2 capture, J. Environ. Chem. Eng. 13 (4) (2025) 117377, https://doi.org/10.1016/j.jece.2025.117377.
[67] M.-K. Kang, S.-B. Jeon, J.-H. Cho, J.-S. Kim, K.-J. Oh, Characterization and comparison of the CO_2 absorption performance into aqueous, quasi-aqueous and non-aqueous MEA solutions, Int. J. Greenh. Gas Control 63 (2017) 281–288, https://doi.org/10.1016/j.ijggc.2017.05.020.
[68] N. El Hadri, D.V. Quang, E.L.V Goetheer, M.R.M Abu Zahra, Aqueous amine solution characterization for post-combustion CO_2 capture process, Appl. Energy 185 (2017) 1433–1449, https://doi.org/10.1016/j.apenergy.2016.03.043.
[69] J.E. Thompson, A.S. Paluch, Revisiting the Clausius/Clapeyron equation and the cause of linearity, Thermo (2023) 412–423, https://doi.org/10.3390/thermo3030025.
[70] I. Kim, H.F. Svendsen, Heat of absorption of carbon dioxide (CO_2) in monoethanolamine (MEA) and 2-(Aminoethyl)ethanolamine (AEEA) solutions, Ind. Eng. Chem. Res. 46 (17) (2007) 5803–5809, https://doi.org/10.1021/ie0616489.
[71] S.H.B. Vinjarapu, T. Regueira, R. Neerup, N. von Solms, P.L. Fosbøl, Heat of absorption of CO_2 in 30 wt% MEA with monoethyleneglycol and urea as vapour reduction additives, Energy 293 (2024) 130609, https://doi.org/10.1016/j.energy.2024.130609.
[72] E.P.J. Linstrom, W.G. Mallard. *NIST Chemistry WebBook, NIST Standard Reference Database Number 69*, 2025. https://doi.org/10.18434/T4D303.